The cume will ask about material as motivated from reading the paper "Evoluation of intrinsic scatter in the SFR-Stellar Mass Correction at 0.5 < Z < 3" by Kurczynski et al. As noted below, you should read single sections at a time, and then answer the questions motivated by that section: you won't need to read the entire paper.

A 70 percent grade will guarantee a pass.

You should be able to answer most of the questions with one or two short statements; you don't need to write long essays!

- 1. (30 points) Read the section "Introduction."
 - (a) (10 points) Galaxy masses.

nitude of both.

- i. What is the difference between the stellar mass of a galaxy and its total mass? Total mass include dark matter (and also gas/dust). Grading: 2 points if dark matter is mentioned, 1 point if only gas/dust is mentioned.
- ii. How might you measure the stellar mass of a galaxy?

 Generally, by measuring luminosity and estimating mass-to-light ratio, e.g., from color, spectrum, or SED. Grading: 2 points for mention of luminosity and something related to mass/light ratio, 1 point for mentioning one but not the other.
- iii. What is a typical range of stellar masses of galaxies, from dwarf galaxies to the most massive galaxies?

 Stellar masses roughly from 10⁶-10¹¹. Grading: 2 points if within one order of

magnitude of both. Graaing: 2 points if within one order

- iv. How might you measure the total mass of a galaxy?

 Generally, using kinematic information, specifically, by measuring a rotation curve (or possibly velocity dispersion profile with modeling); gravitational lensing would be another possibility, but with somewhat limited applicability. Grading: 2 points for mentioning rotation curves, 1 point for some vaguer mention of kinematics.
- v. What is a typical range of total masses of galaxies, from dwarf galaxies to the most massive galaxies?
 Total masses roughly from 10⁷-10¹². Grading: 2 points if within one order of mag-
- (b) (10 points) The paper discusses the "main sequence" of star forming galaxies. However, star forming galaxies only comprise a fraction of current day galaxies. Sketch a color vs. absolute magnitude diagram of galaxies, labelling the axes including numerical values (you can choose whatever bandpasses you like, but you need to label what the axes are!). Put points on the diagram representing galaxies in the local universe; try to make the point density representative of the relative numbers of galaxies. Identify the location of the star forming galaxies.

Looking for a diagram that covers an appropriate range of color and absolute magnitudes for galaxies, a recognition that there is a red and a blue sequence, and that the blue sequence corresponds to star forming galaxies. Grading: 2 points for reasonable axis labels, 3 points for bimodality, 3 points for luminosity function consideration, 2 points for locating star forming galaxies.

- (c) (5 points) What does it mean when the paper says: "Magnitudes are in the AB system"? AB system is where magnitude is $-2.5 \log F_{\nu} + const$, ideally giving value of constant (such that Vega is 0).
- (d) (5 points) What does it mean when the paper says: "we use the cosmology $\Omega_{\Lambda} = 0.7$, $\Omega_0 = 0.3$ and $H_0 = 70$ km/s/Mpc", i.e. what do each of these terms mean? Ω_{Λ} is dark energy density, Ω_0 is matter density (dark + baryonic), and H_0 is present day Hubble constant; densities are expressed as a fraction of the critical density. Grading: 2 points for Hubble constant, 4 points if Ω_{Λ} is only associated with cosmological constant (as opposed to dark energy).
- 2. (10 points) Read the section "Data and sample selection"
 - (a) (6 points) What is the difference between a spectroscopic redshift, a grism redshift, and a photometric redshift?
 - Spectroscopic redshift gets redshift from emission lines, grism redshift is lower dispersion spectrum where you might get the reshift from an emission line or from the SED (at lower precision that spectroscopic), and photometric redshift determine from simultaneously fitted intrinsic SED and redshift to a set of photometry in different bandpasses (at even lower precision). Grading: 2 points for each term.
 - (b) (4 points) What range of wavelength is covered by the 17 band CANDELS photometry (U band through IRAC)? Note that IRAC is a mid-IR instrument on the Spitzer Space Telescope.
 - U band is ~ 3500 Å, and longest IRAC band is $\sim 8\mu$. Grading: 2 points for being close on one end.
- 3. (35 points) Read the section "Method"
 - (a) (5 points) What is a Markov Chain Monte Carlo analysis, and what would it provide in the context of the application in the paper?
 - Numerical method for sampling a probability distribution function, often used in the context of Bayesian analysis of a problem. Specifically, one starts at some location in parameter space and evaluates the probability, then chooses steps from the previous position that are devised such that the steps eventually sample the underlying probability distribution. In this application, it would provide the joint (or marginal) probability distributions of the four parameters.
 - (b) (20 points) Note that this question is not directly related to the paper! Imagine you were fitting the spectral energy distribution (SED) of a star to estimate its temperature. You are provided the following table of observations, and best fit results for 3 model spectra with parameters (temperature/mass combination) as specified in the table:

Wavelength	Model A: 4000 K	Model B: 5000 K	Model C: 6000 K	Observed with uncertain
	mass: 0.6 Msun	mass: 0.82 Msun	mass: 1.05 Msun	
4000	13.08	12.62	12.31	12.36+/- 0.25
5000	11.85	11.78	11.73	11.79+/- 0.25
6000	11.14	11.32	11.44	11.24+/- 0.25
7000	10.71	11.07	11.31	11.40+/- 0.25

The models have been individually offset (fit) to provide the best fits (one degree of freedom).

- i. Write the expression for χ^2 . Using a standard χ^2 analysis, quantitatively determine which model provides the best fit.

 Calculate χ^2 for each model properly: $\chi^2(A) = 16.13 \ \chi^2(B) = 2.92 \ \chi^2(C) = 0.87$ determine model C is best fit. Grading: 2 points for getting model C, 3 points for correct definition and calculation of χ^2
- ii. Say you know that this star is in a young star cluster, where the number of stars as a function of their mass is given by a Salpeter initial mass function $(dn/dM \propto M^{-2.35})$. In the absence of any other observations (i.e., without the observed column in the table above), which of the three models would you expect to be the most likely, or would you expect them to all be equally likely? Quantitatively give the relative probabilities of the three models.

Without any additional information, model A is most probable because there are more low mass stars, with probability in proportion to $M^{-2.35}$ For M=0.6,0.82,1.05, I get P=3.73:1.79:1, or, normalized, P=0.57:0.27:0.15 Grading: 4 points for recognizing that lower mass stars are more likely, 5 points for getting probabilities.

iii. Write the expression for the Bayesian analysis that would determine the probability of each model given the observations and the knowledge that the star is in a young star cluster where the mass function is well-represented by a Salpeter function. Make sure to define the terms in your expression.

$$P(M|D) \propto P(D|M)P(M)$$

where P(D|M) is the relatively probability of each model given the observations, (i.e., the relative probabilities for the various χ^2 values), and P(M) is the prior probability of each model, determined here from the IMF (i.e. $M^{-2.35}$). Grading: 4 points for correct Bayesian expression, 5 points for associating terms with the problem.

iv. The following table gives the probabilities (bottom row) of having χ^2 larger than the values specified in the rows for various degrees of freedom (DOF).

DOF	χ^2 values										٠.
1	0.004	0.02	0.06	0.15	0.46	1.07	1.64	2.71	3.84	6.64	10.83
2	0.10	0.21	0.45	0.71	1.39	2.41	3.22	4.60	5.99	9.21	13.82
3	0.35	0.58	1.01	1.42	2.37	3.66	4.64	6.25	7.82	11.34	16.27
Probability	0.95	0.90	0.80	0.70	0.50	0.30	0.20	0.10	0.05	0.01	0.001

Using your previous χ^2 values, combined with the prior probabilities from the initial mass function, to quantitatively determine which model is the most likely. (If you don't think you have reasonable χ^2 values from above, adopt values of 15, 3, and 1 for models A, B, and C, respectively.)

$$P(\chi^2 > 2.92) \sim 0.15$$

 $P(\chi^2 > 0.87) \sim 0.6$
 $P(M = 0.82)/P(M = 1.05) = 1.8$

considering relative probabilities, looks like model C is still the most likely.

- (c) (5 points) Why do the authors choose a value of $\chi^2 > 50$ to reject SEDs? Describe both why they reject fits with large χ^2 and also why they might have chosen the value of 50. Fits with large χ^2 will likely bias estimates of intrinsic scatter. As for why $\chi^2 > 50$, note that fits have 13 degrees of freedom, so this corresponds to $\chi^2_{\nu} < \sim 4$ (not that this is any magic number!).
- (d) (5 points) The authors note that their SFRs are less sensitive to short timescale variations than spectroscopic (Hα) indicators. Why is this, i.e., what sets the timescale for a SFR indicator that is based on Hα vs one that is based on spectral energy distribution?
 Hα arises only when stars that produce ionizing radiation are present, i.e. hotter than mid-B stars, which have a lifetime of a few tens of millions of years only. SED fitting relies on continuum shape, which is affected by stars of all temperatures, weighted by number of stars and luminosity at each temperature.
- 4. (10 points) Read the section "Results"
 - (a) (5 points) The authors note that the intercept of the stellar mass-SFR relation decreases with cosmic time. What does this imply about the history of star formation in the Universe?
 - Decreasing star formation rate over the range of redshifts studied.
 - (b) (5 points) The authors note that the intrinsic scatter in the relation appears to increase with cosmic time. What is the implication of this? More bursty at later times.
- 5. (5 points) Treatment of Uncertainties: read just the first paragraph!
 - (a) (5 points) Describe in your own terms what covariances are in the context of these model fits.

Covariances are when uncertainties or parameters are correlated (or anti-correlated) with each other, i.e. comparably good fits are found for different combinations of parameters. Grading: 5 points if correlations between parameters are mentioned, 3 points if less specific.



EVOLUTION OF INTRINSIC SCATTER IN THE SFR-STELLAR MASS CORRELATION AT 0.5 < z < 3

Peter Kurczynski¹, Eric Gawiser¹, Viviana Acquaviva², Eric F. Bell³, Avishai Dekel⁴, Duilia F. de Mello^{5,6}, HENRY C. FERGUSON⁷, JONATHAN P. GARDNER⁵, NORMAN A. GROGIN⁷, YICHENG GUO⁸, PHILIP F. HOPKINS^{9,10},
ANTON M. KOEKEMOER⁷, DAVID C. KOO⁸, SEONG-KOOK LEE¹¹, BAHRAM MOBASHER¹², JOEL R. PRIMACK¹³,

MARC RAFELSKI^{5,15}, EMMARIS SOTO^{5,6}, AND HARRY I. TEPLITZ¹⁴

1 Department of Physics and Astronomy, Rutgers University, Piscataway, NJ 08854, USA

2 Now York Civ. College of Technology, Purplies NV 11504

New York City College of Technology, Brooklyn, NY 11201, USA ³ Department of Astronomy, University of Michigan, Ann Arbor, MI 48109, USA

⁴ Center for Astrophysics and Planetary Science, Racah Institute of Physics, The Hebrew University, Jerusalem 91904, Israel ⁵ Laboratory for Observational Cosmology, Astrophysics Science Division, NASA Goddard Space Flight Center, Code 665, Greenbelt, MD 20771, USA Department of Physics, The Catholic University of America, Washington, DC 20064, USA

Space Telescope Science Institute, 3700 San Martin Drive, Baltimore, MD 21218, USA 8 UCO/Lick Observatory, Department of Astronomy and Astrophysics, University of California, Santa Cruz, CA, USA TAPIR, California Institute of Technology, Mailcode 350-17, Pasadena, CA 91125, USA

¹⁰ Department of Astronomy and Theoretical Astrophysics Center, University of California, Berkeley, CA 94720, USA 11 Center for the Exploration of the Origin of the Universe, Department of Physics and Astronomy, Seoul National University, Seoul 151-742, Korea Department of Physics and Astronomy, University of California, Riverside, CA, USA

Department of Physics, University of California, Santa Cruz, CA 95064, USA ¹⁴ Infrared Processing and Analysis Center, Caltech, MS 100-22, Pasadena, CA 91125, USA Received 2015 November 16; accepted 2016 February 15; published 2016 March 14

ABSTRACT

We present estimates of intrinsic scatter in the star formation rate (SFR)-stellar mass (M_*) correlation in the redshift range 0.5 < z < 3.0 and in the mass range $10^7 < M_* < 10^{11} M_{\odot}$. We utilize photometry in the Hubble Ultradeep Field (HUDF12) and Ultraviolet Ultra Deep Field (UVUDF) campaigns and CANDELS/GOODS-S and estimate SFR, M* from broadband spectral energy distributions and the best-available redshifts. The maximum depth of the UDF photometry (F160W 29.9 AB, 5σ depth) probes the SFR- M_* correlation down to $M_* \sim 10^7 M_{\odot}$, a factor of $10-100 \times$ lower in M_* than previous studies, and comparable to dwarf galaxies in the local universe. We find the slope of the SFR-M* relationship to be near unity at all redshifts and the normalization to decrease with cosmic time. We find a moderate increase in intrinsic scatter with cosmic time from 0.2 to 0.4 dex across the epoch of peak cosmic star formation. None of our redshift bins show a statistically significant increase in intrinsic scatter at low mass. However, it remains possible that intrinsic scatter increases at low mass on timescales shorter than ~100 Myr. Our results are consistent with a picture of gradual and self-similar assembly of galaxies across more than three orders of magnitude in stellar mass from as low as $10^7 M_{\odot}$

Key words: galaxies: dwarf - galaxies: evolution - galaxies: formation - galaxies: high-redshift galaxies: statistics

1. INTRODUCTION

A central issue in understanding how galaxies form is whether star formation is a gradual, continuous process or whether it happens in bursts. The widely reported correlation between star formation rate (SFR) and stellar mass (M_*) in starforming galaxies ("main sequence"; e.g., Daddi et al. 2007; Noeske et al. 2007; Salim et al. 2007; Wuyts et al. 2011) provides an observational means to address this issue. Because M_{*} is related to past-average SFR, the small total observed scatter around this correlation (~ 0.3 dex at $z \lesssim 2$; Behroozi et al. 2013) suggests gradual assembly of stellar mass, as opposed to bursty star formation.

Bursty star formation introduces scatter to the SFR-M* relation and diversity to star formation histories (e.g., Abramson et al. 2014); it is found to dominate the evolution of low-mass galaxies in simulations (Shen et al. 2014; Domínguez et al. 2015) and in observations of local galaxies (e.g., Kauffmann 2014; Weisz et al. 2014; Benítez-Llambay et al. 2015). In particular, McOuinn et al. (2010) find starbursts in dwarf galaxies to occur with durations in the 100 Myr-1 Gyr range that will be probed here. Furthermore, stochasticity in star formation may arise at low SFR values due to sampling effects (Fumagalli et al. 2011; da Silva et al. 2012, 2014).

Guides to the extensive SFR-M* literature can be found in Behroozi et al. (2013) and Speagle et al. (2014). Studies to date have not modeled scatter. The typically reported total observed scatter includes SFR and M* measurement uncertainties and covariances as well as the underlying intrinsic scatter.16 However, cosmological galaxy evolution simulations make predictions for the physically meaningful quantity, intrinsic scatter, which in the absence of measurement errors and covariances, is the standard deviation (dex) of the SFR- M_* fit residuals. In this Letter, we present an analysis of the SFR- M_* relation that specifically addresses intrinsic scatter.

To probe SFR- M_* to the lowest possible mass, we utilize photometry from the Hubble Space Telescope (HST) in the Hubble Ultradeep Field (HUDF; Beckwith et al. 2006), including HUDF12 (Ellis et al. 2013; Koekemoer et al. 2013; see also Illingworth et al. 2013), UVUDF (Teplitz et al. 2013), and the Cosmic Assembly Near-infrared Deep Extragalactic Legacy Survey (CANDELS; Grogin et al. 2011; Koekemoer

¹⁵ NASA Postdoctoral Program Fellow.

¹⁶ Salmon et al. (2015) and Shivaei et al. (2015) do compute intrinsic scatter post-hoc from fit residuals, without covariances or estimated uncertainties to the intrinsic scatter.

et al. 2011). Magnitudes are in the AB system; we use the cosmology $\Omega_{\Lambda}=0.7$, $\Omega_{0}=0.3$, and $H_{0}=70\,\mathrm{km\,s^{-1}\,Mpc^{-1}}$

2. DATA AND SAMPLE SELECTION

We form samples of galaxies for analysis from CANDELS GOODS-S and UVUDF photometric catalogs. We utilize the selection criteria of Santini et al. (2015) to reject poor quality data, stars, and active galactic nuclei. We utilize exceptionally deep HUDF photometry since our primary motivation is to probe to low mass, while the larger, complementary CANDELS data provide overlapping and continuous coverage of the mass range up to $\sim 10^{11} M_{\odot}$. Notably, the HUDF photometry enables detecting dwarf galaxies with $M_* \sim 10^7 M_{\odot}$ at z > 0.5 (compare with the Small Magellanic Cloud, $M_* \sim 10^8 M_{\odot}$).

We select sources in the redshift range $0.5 < z \le 3.0$, including 2444 spectroscopic redshifts. In the larger CANDELS catalog, we require spectroscopic redshifts; crosslistings in the smaller UVUDF catalog (Rafelski et al. 2015) use grism (3D-HST; Skelton et al. 2014) or photometric redshifts. UVUDF photometric redshifts have fewer outliers than CANDELS photometric redshifts (Rafelski et al. 2015). Using the best-available redshifts is preferable for estimating scatter; see Section 4. We form samples in five redshift bins $0.5 < z \le 1.0$, $1.0 < z \le 1.5$, $1.5 < z \le 2.0$, $2.0 < z \le 2.5$, and $2.5 < z \le 3.0$ that have 1369, 1100, 673, 439, and 435 sources, respectively.

We use 17 bands from the CANDELS photometry (U-band through IRAC; Guo et al. 2013) to generate input data for fits to the spectral energy distributions (SEDs), which are used to estimate physical parameters such as SFR and M_{\star} .

3. METHOD

We fit SEDs with a Markov Chain Monte Carlo based program (Acquaviva et al. 2011, 2012) to estimate SFR, M_* , E(B-V) (spectral reddening), age, and star formation history timescale, τ (discussed below). Age varies from 1 Myr to the age of the universe at each (binned) galaxy redshift. Ages are found to fall between ~100 Myr and 1 Gyr, with no ages younger than 10 Myr; however, the 1 Myr lower limit was found to improve χ^2 for several sources compared to a more stringent 10 Myr lower limit.

Galaxy mass varies between 10^4 and $10^{15}M_{\odot}$; E(B-V) varies from 0.01 to 0.99. τ is sampled logarithmically from 0.02 to 4.99 Gyr. We use the Bruzual & Charlot (2003) stellar templates, including nebular emission lines; the Salpeter (1959) initial mass function (IMF); and the Calzetti et al. (2000) dust attenuation law. Metallicity is fixed at $Z=0.2Z_{\odot}$; fits at solar metallicity have generally poor convergence and larger parameter uncertainties. We utilize parameter uncertainties and covariances for each galaxy.

We explore several continuous star formation histories including constant, linear, exponential (" τ model"), and linear-exponential ("delayed τ model"). The linear-exponential model (Lee et al. 2010) permits both rising and falling star formation and yields comparable median χ^2 values as the next best model (exponential). We report results obtained with this model and estimate its parameters, τ_0 (time-to-peak) and τ (decay timescale). Instantaneous SFRs are most sensitive to star formation within \sim 100's Myr before observation. These SFRs are less sensitive to short timescale (e.g., 10 Myr) variations

than spectroscopic indicators ($H\alpha$) and yield lower scatter than them (Hopkins et al. 2014; Domínguez et al. 2015).

We reject SEDs with bad fits ($\chi^2 > 50$; 263, 229, 186, 158, and 80 galaxies in each redshift bin, respectively) or poor convergence (GR >0.2; Gelman & Rubin 1992; 131, 95, 55, 62, and 30 galaxies). SED fits with large χ^2 values have potentially underestimated parameter uncertainties that overestimate scatter. Our final redshift-binned samples have 958, 692, 466, 246, and 326 galaxies for SFR- M_* analysis.

For each sample, we fit log SFR and $\log M_*$ values to the model:

$$\log SFR = a \times \log M_* + b + N(0, \sigma_{IS}). \tag{1}$$

The parameters a and b describe the linear relationship and the Gaussian random variable, $N(0, \sigma_{\rm IS})$, with zero mean, and unknown standard deviation, $\sigma_{\rm IS}$, describes intrinsic scatter. We use the analytic method of Fuller (1987, hereafter F87) to estimate parameters in the presence of uncertainties and covariances. A full-width tenth maximum clipping range is obtained from the histogram of initial fit residuals to exclude outliers (our results are insensitive to the details of clipping). We re-fit the outlier-clipped data to estimate the model parameters.

4. RESULTS

Results include estimated parameters for five redshift-binned samples spanning the mass range $10^7 \lesssim M_* \lesssim 10^{11} M_\odot$. Figure 1 shows the SFR versus M_* data and fits; we find significant correlations (Pearson r^2 values in the range 0.66–0.81). We compare with Whitaker et al. (2014) ¹⁸ over their redshift range 0.5 < z < 2.5 and the meta-analysis of Speagle et al. (2014).

Figure 2 shows that residuals do not suggest deficiencies in the model or the fits: the band of residuals clusters around zero (suggestive of a good fit) and does not curve with M_* (higher-order model is not needed). We find more negative residuals than positive residuals due to an age-gradient effect: age decreases toward the upper left in Figure 1, roughly perpendicular to the best-fit line. Consequently, there is a sharp upper cutoff in the locus of galaxies as age diminishes toward zero; older galaxies are found below and to the right.

The distributions of total scatter of the mass-binned residuals are indicated in the bottom panels of Figure 2. Box plots indicate the inter-quartile ranges, and red lines indicate the medians, which are near zero.

The estimated parameters are shown in Figure 3 and Table 1. We detect intrinsic scatter in all redshift bins; scatter increases with cosmic time from the highest-redshift bin to the lowest bin, from 0.220 dex to 0.427 dex for intrinsic scatter and 0.369 dex to 0.525 dex for total scatter, respectively. The estimated slope is near unity, and we find the intercept to decrease with cosmic time, similar to trends found in Whitaker et al. (2014).

We do not find the turnover in slope above $\log M_* \sim 10 M_\odot$ that has been previously reported (Lee et al. 2015); our study, aimed at low mass, has small number statistics above $\log M_* > 10.5$. Below $\log M_* \sim 8.0$, we continue to find a linear trend.

Table 2 shows intrinsic and total scatter in mass-binned subsamples. For each subsample, the linear model parameters

 $^{^{17}}$ A small effect; rejecting $\chi^2 > 100$ increases scatter by ~10%.

Adjusted upward by a factor of $\log_{10}(1.8)$ to convert from their adopted Chabrier (2003) IMF to the Salpeter (1959) IMF used here.

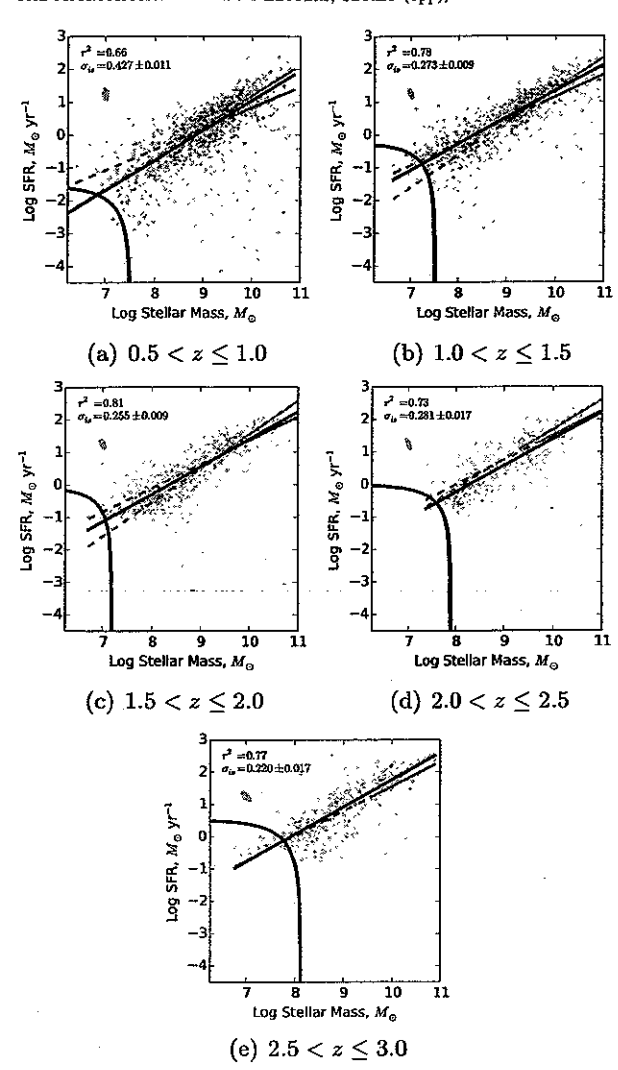


Figure 1. Star formation rate vs. stellar mass (M_*) in the redshift range 0.5 < z < 3.0 for galaxies in a combined CANDELS (spec-z) and UVUDF (photo-z) sample. In the $0.5 < z \le 1.0$ bin, seven outliers with log SFR < -3 are not shown. Outliers (red points) from an initial fit are clipped; remaining galaxies (gray points) are used to determine the best fit (dark purple). Results from Whitaker et al. (2014; cyan) and the meta-analysis of Speagle et al. (2014; red) are shown; dashed regions indicate extrapolations from their reported ranges in M_* . Selection curves are shown in black; our data are insensitive to galaxies that would fall to the lower left of each curve. The squared Pearson correlation coefficient, r^2 , and estimated intrinsic scatter, σ_{1S} (dex), are indicated by the text label. A typical error ellipse is shown in the upper left, with half-width and half-height equal to the median error in $\log M_*$ and \log SFR, respectively, and orientation determined by the median covariance.

are pinned and only the intrinsic scatter is estimated. At each redshift, the total scatter is relatively constant across the mass range; it is smallest at low mass, and relatively constant or somewhat increasing toward higher mass. The scatter does not increase in the lowest-mass bin, which is particularly surprising because, as mentioned above, scatter in SFR- M_* is greater at low mass in local dwarf galaxies, and also in simulations. Because scatter is associated with bursty star formation, these results suggest that at $\log M_* \sim 7$, we do not see a significant increase in burstiness compared to higher masses.

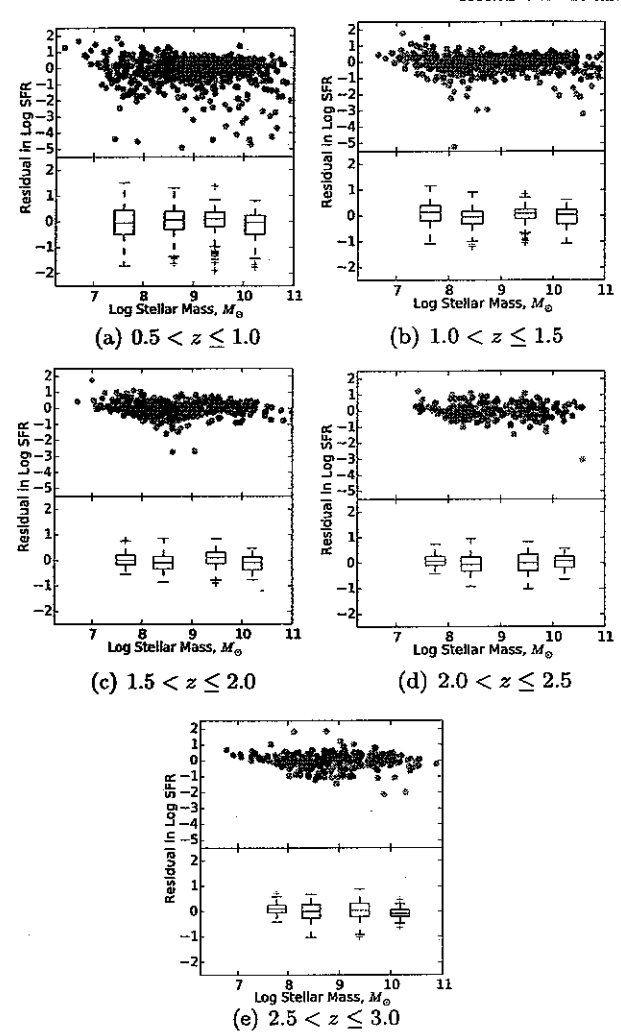


Figure 2. Residuals to fits of star formation rate (SFR) vs. stellar mass (M_*) shown in Figure 1. (Upper panels) Residuals from initial fit are shown as blue circles, with outliers in red. (Lower panels) Residuals are analyzed in four bins of stellar mass $(<10^8, 10^8, 10^9, 10^9, 10^9-10^{10}, >10^{10} M_{\odot})$. Box heights and whiskers indicate inter-quartile ranges (IQRs) and $1.5 \times IQR$ of the residuals in each bin. Median residual is indicated by the red lines within each box, and horizontal box placement is at the median stellar mass of each bin.

5. TREATMENT OF UNCERTAINTIES

Our analysis incorporates covariances between SED fit parameters, which are non-negligible. Median, correlated SFR and M_* uncertainties are indicated as error ellipses in Figure 1. M_* uncertainties increase toward lower mass; SFR uncertainties and covariances exhibit no trend with mass. SFR tends to be anti-correlated with M_* , e.g., the $1.0 < z \le 1.5$ SFR- M_* correlation has mean = -0.46. Neglecting covariances overestimates intrinsic scatter by $\sim 5\%-10\%$, whereas slope and intercept estimates are not significantly affected.

Uncertainties to SFR- M_* model parameters are determined by simulation. Random realizations are formed from the best-fit model; additional Gaussian random noise and intrinsic scatter are added. Simulations have 1000 realizations, and use the same analysis as on the observed data. Uncertainties are given by the standard deviations of the resulting true error distributions.

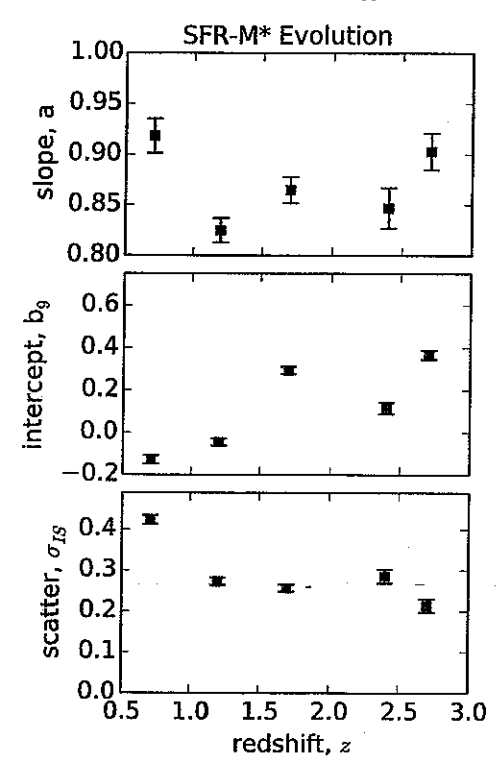


Figure 3. Estimated model parameters for the log SFR-log M_* relationship analyzed in five redshift bins in the range $0.5 < z \leqslant 3.0$. Slope (top panel) and intercept (middle panel) refer to the linear components of the model, with M_* values scaled to $10^9 M_{\odot}$. The width, σ , of the Gaussian intrinsic scatter is shown in the bottom panel, in units of dex. Errors to the model parameters are computed from simulations.

To assess systematics, we use several fitting methods. We use ordinary least squares (OLS), weighted least squares (χ^2 minimization), and orthogonal distance regression (ODR), although they do not use the fully available uncertainties and covariances or estimate intrinsic scatter. We also implement methods that estimate intrinsic scatter (Tremaine et al. 2002; Kelly 2007) or account for it (Akritas & Bershady 1996).

We separately compute the intrinsic scatter variance, σ_{1S}^2 , from the fit residuals. The scatter, $\langle \sigma_T^2 \rangle$ (where $\langle \rangle$ denotes the sample mean), the $\log M_*$ and \log SFR errors, σ_X , σ_Y , respectively, the covariance, Cov(X, Y), and slope, a, are related as

$$\sigma_{\rm IS}^2 = \langle \sigma_T^2 \rangle - \langle \sigma_Y^2 \rangle - a^2 \langle \sigma_Y^2 \rangle + 2a \langle {\rm Cov}(X, Y) \rangle. \tag{2}$$

We implement this computation for methods that do not explicitly model scatter. For large scatter, we find excellent agreement between methods (e.g., less than 2% variation for $\sigma_{\rm IS} \sim 0.24$), and at low intrinsic scatter we find significant dispersion (e.g., 66% variation for $\sigma_{\rm IS} \sim 0.08$).

To determine the systematic effect of spectroscopic redshift selection, we analyze an independent sample of number-matched photometric redshift sources from CANDELS (combined with the UVUDF sources) in the range $1.0 < z \le 1.5$. We find that total scatter and outlier fractions are unchanged. However, intrinsic scatter is reduced in the photometric sample by $\sim 35\%$ in methods without covariances and $\sim 60\%$ in methods that use covariances. The total scatter is unchanged in

the photometric sample, whereas the less-accurate photometric redshifts increase the scatter due to M_{*} . Thus, reduced intrinsic scatter in the photometric sample follows from Equation (2); the remaining variance in the "scatter budget" available to intrinsic scatter is reduced. This observation affirms our using the best-available photometric redshifts.

We investigate whether our results may be biased by incompleteness. We pay particular attention to low-mass galaxies ($\log M_* \lesssim 9$) that are detected predominantly in UVUDF and for which mass incompleteness sets in at z > 1in CANDELS data. The UVUDF detection image is an average of eight wavebands from F435W redward to F160W, and therefore has a complex selection function. To approximate this function in the SFR-M* plane, we use a UVUDF flux density threshold corresponding to magnitude 29.0 in the detection image. We use SED model parameters to express this detection threshold in terms of SFR and M_* ; these selection functions are shown as black curves in Figure 1. We are insensitive to galaxies below and to the left of these curves. We cannot rule out the possibility of extremely passive galaxies far from the SFR-M* correlation from having been missed; however, such galaxies would be excluded from our analysis as outliers. Thus, our results are robust to this incompleteness. However, above z > 2, these curves suggest that scatter estimates at low mass are significantly affected by incompleteness.

We also investigate the dependence of our results upon the assumed form of the star formation history. We completed analyses with SED fit parameters obtained from constant and exponential star formation histories in addition to the linear-exponential model. For example, at $1.0 < z \le 1.5$, intrinsic scatter is 0.13, 0.20, and 0.28 dex for the constant, linear-exponential, and exponential star formation histories, respectively. Thus, varying star formation history reveals a systematic uncertainty of ± 0.08 , with constant star formation history leading to the lower value and the exponentially declining leading to the higher value; the true systematic uncertainty may be less given the unphysical assumptions of the alternate star formation histories.

As with any parameter estimation, the fidelity of our results depends upon the efficacy of the model, which in the present case includes the assumed form of the star formation history. We adopt the linear-exponential model because of its flexibility and good SED fits compared to available alternatives. A logical extension of this work would be to include more complex star formation histories that include multiple bursts (our preferred, linear-exponential model effectively accommodates a single, initial burst) and determine from simulation the extent to which the data can discriminate between alternatives.

6. CONCLUSION

These results extend the study of the SFR- M_* relationship of star-forming galaxies in the redshift range $0.5 < z \le 3$ by more than an order of magnitude in stellar mass. This lowermass limit of $\sim 10^7 \, M_\odot$ is comparable to dwarf galaxies in the local universe. We use SED fitting to estimate SFR and M_* as well as their uncertainties and covariances. Where measurable, we find the intrinsic scatter to be a substantial fraction ($\gtrsim 50\%$) of the total scatter. We find the intrinsic scatter to be $\sigma_{\rm IS} \approx 0.2$ –0.4 dex; see Tables | and 2. These values are somewhat larger than the simulations of Dutton et al. (2010), who find $\sigma = 0.11$ dex at $z \sim 0$, but are in good agreement

Table 1
Linear Plus Intrinsic Scatter Model Parameters

Redshift (1)	N (2)	<i>a</i> (3)	<i>b</i> (4)	<i>b</i> ₉ (5)	σ _{int} (6)	σ_{Tot} (7)
$0.5 < z \le 1.0$	913	0.919 ± 0.017	-8.394 ± 0.011	-0.121 ± 0.021	0.427 ± 0.011	0.525
$1.0 < z \le 1.5$	671	0.825 ± 0.012	-7.474 ± 0.010	-0.045 ± 0.016	0.273 ± 0.009	0.383
$1.5 < z \le 2.0$	447	0.867 ± 0.013	-7.484 ± 0.011	0.321 ± 0.017	0.255 ± 0.008	0.354
$2.0 < z \le 2.5$	237	0.849 ± 0.021	-7.513 ± 0.018	0.128 ± 0.028	0.281 ± 0.017	0.399
$2.5 < z \leqslant 3.0$	304	0.899 ± 0.017	-7.729 ± 0.015	0.367 ± 0.023	0.220 ± 0.017	0.369

Note. (1) Redshift range of the sample. (2) Number of galaxies in the final fit (excluding outliers). (3, 4, 6) Estimated parameters of the model $\log SFR = a \log M_* + b + N(0, \sigma_{\rm int})$ including SFR and M_* uncertainties and covariances. (5) Intercept, b_9 , corresponds to the mass-scaled model $\log SFR = a(\log M_* - 9.0) + b_9$ in which errors to the fit parameters are approximately uncorrelated. (7) Total scatter, defined as sample standard deviation of the fit residuals after clipping of outliers.

Table 2
Scatter about the SFR-M* Relation for Galaxies in CANDELS/UVUDF in Bins of Stellar Mass and Redshift

Statistic	$6 < \log M_* \leqslant 8$	$8 < \log M_* \leqslant 9$	$9 < \log M_* \leqslant 10$	$10 < \log M_* \leqslant 1$
		$0.5 < z \le 1.0$		
Num Galaxies	128	298	430	102
Intr. scat., dex	0.462 ± 0.030	0.404 ± 0.012	0.315 ± 0.011	0.435 ± 0.026
Total scat., dex	0.552	0.445	0.368	0.428
Outlier fraction +	0.031	0.000	0.000	0.000
Outlier fraction -	0.156	0.067	0.074	0.176
		$1.0 < z \leqslant 1.5$		
Num. galaxies	111	209	284	87
Intr. scat., dex	0.201 ± 0.025	0.249 ± 0.010	0.230 ± 0.006	0.281 ± 0.014
Total scat., dex	0.315	0.285	0.285	0.348
Outlier fraction +	0.027	0.000	0.000	0.000
Outlier fraction -	0.009	0.053	0.004	0.103
		$1.5 < z \leqslant 2.0$		
Num. galaxies	99	189	144	30
Intr. scat., dex	0.279 ± 0.022	0.497 ± 0.018	0.332 ± 0.008	0.417 ± 0.025
Total scat., dex	0.406	0.437	0.340	0.348
Outlier fraction +	0.000	0.000	0.000	0.000
Outlier fraction -	0.000	0.005	0.007	0.000
		2.0 < z ≤ 2.5		
Num. galaxies	29	111	85	18
Intr. scat., dex	0.232 ± 0.050	0.337 ± 0.027	0.425 ± 0.022	0.240 ± 0.048
Total scat., dex	0.354	0.451	0.491	0.308
Outlier fraction +	0.000	0.000	0.000	0.000
Outlier fraction -	0.000	0.000	0.000	0.053
		$2.5 < z \leqslant 3.0$		
Num. galaxies	50	146	106	-23
Intr. scat., dex	$< 0.03(3\sigma)$	0.421 ± 0.018	0.392 ± 0.019	0.309 ± 0.069
Total scat., dex	0.267	0.516	0.464	0.331
Outlier fraction +	0.000	0.000	0.000	0.000
Outlier fraction -	0.000	0.000	0.009	0.042

Note. The number of galaxies in each bin is tabulated, and the intrinsic scatter is estimated with the method of F87 with errors determined from simulation. The total scatter (standard deviation of residuals to the linear fit) is tabulated for comparison. Outlier fraction +(-) refers to the fraction of sources in each bin above (below) the initial best-fit line that are clipped and excluded from the final fit.

with the Illustris simulations in the overlapping mass range $M_* > 10^8 M_{\odot}$ below $z \le 2$ (Sparre et al. 2015b). We encourage modelers to report their observables to even lower mass for comparison with these observations.

We find the intrinsic scatter in the SFR- M_* relation to increase with cosmic time (decreasing redshift) by about a factor of two across the range 2.5 > z > 0.5, although most of this increase occurs for a single redshift bin, $0.5 < z \le 1.0$.

Increasing scatter with cosmic time is also found in the models of Somerville et al. (2015) and Sparre et al. (2015b).

At each redshift, we find the scatter to be relatively constant (or slightly decreasing) toward lower mass, particularly above z>1, in disagreement with trends for broadband SFR reported in the theoretical studies of Domínguez et al. (2015) and Sparre et al. (2015a). These studies each report substantially larger scatter at low masses for H α -based SFRs than the broadband ones used here. SED fitting is sensitive to $\gtrsim 100$ Myr timescale variability, while spectroscopic indicators are needed for shorter time variability. We interpret the absence of increased scatter to mean that such intermediate or long timescale variability does not dominate the star formation histories of low-mass galaxies.

Without specifically addressing the timescale issue, the simulations of Somerville et al. (2015), predict a moderate increase in scatter toward low mass in the range $M_* > 10^8 \, M_\odot$ over our redshift range, whereas the simulations of Sparre et al. (2015b) and Dutton et al. (2010) show constant scatter with mass down to $M_* = 10^9$ and $M_* = 10^3 M_\odot$, respectively. In these simulations, SFR is computed from molecular hydrogen gas density and empirically motivated models of subgrid physics.

The origin of the confinement of star-forming galaxies to a narrow SFR- M_* correlation is a theoretical question of major interest (e.g., Dutton et al. 2010; Rodriguez-Puebla et al. 2015; Tacchella et al. 2016 and references therein). Tacchella et al. (2016) show that it could be understood in terms of the evolution of galaxies through phases of gas compaction, depletion, possible replenishment, and eventual quenching. In any case, the low scatter we observe in SFR suggests a remarkable consistency in star formation spanning 3-4 orders of magnitude in galaxy stellar mass. It invites comparison with other dynamical systems across a variety of disciplines from physics to biology where power-law scaling relations are associated with self-regulating dynamics.

The authors wish to thank Aaron Clauset for discussions. Support for *HST* Program GO-12534 was provided by NASA through grants from the Space Telescope Science Institute. This material is based upon work supported by the National Science Foundation under grant No. 1055919. This work is based on observations taken by the CANDELS Multi-Cycle Treasury Program with the NASA/ESA *HST*, which is operated by the Association of Universities for Research in Astronomy, Inc., under NASA contract NAS5-26555.

REFERENCES

Abramson, L. E., Kelson, D. D., Dressler, A., et al. 2014, ApJL, 785, L36 Acquaviva, V., Gawiser, E., & Guaita, L. 2011, ApJ, 737, 47

Acquaviva, V., Gawiser, E., & Guaita, L. 2012, IAU Symp. 284, The Spectral Energy Distribution of Galaxies, ed. R. J. Tuffs, & C. C. Popescu (Cambridge: Cambridge Univ. Press), 42 Akritas, M. G., & Bershady, M. A. 1996, ApJ, 470, 706 Beckwith, S. V. W., Stiavelli, M., Koekemoer, A. M., et al. 2006, AJ, Behroozi, P. S., Wechsler, R. H., & Conroy, C. 2013, ApJ, 770, 57 Benéz-Llambay, A., Navarro, J. F., Abadi, M. G., et al. 2015, MNRAS, 450, 4207 Bruzual, G., & Charlot, S. 2003, MNRAS, 344, 1000 Calzetti, D., Armus, L., Bohlin, R. C., et al. 2000, ApJ, 533, 682 Chabrier, G. 2003, PASP, 115, 763 da Silva, R. L., Fumagalli, M., & Krumholz, M. 2012, ApJ, 745, 145 da Silva, R. L., Fumagalli, M., & Krumholz, M. R. 2014, MNRAS, 444. 3275 Daddi, E., Dickinson, M., Morrison, G., et al. 2007, ApJ, 670, 156 Domínguez, A., Siana, B., Brooks, A. M., et al. 2015, MNRAS, 451. 839 Dutton, A. A., van den Bosch, F. C., & Dekel, A. 2010, MNRAS, Ellis, R. S., McLure, R. J., Dunlop, J. S., et al. 2013, ApJL, 763. L7 Fuller, W. 1987, Measurement Error Models (New York: Wiley) Fumagalli, M., da Silva, R. L., & Krumholz, M. R. 2011, ApJL, 741, L26 Gelman, A.; & Rubin, D. B. 1992, Statistical Science, 7, 457 Grogin, N. A., Kocevski, D. D., Faber, S. M., et al. 2011, ApJS, 197, 35 Guo, Y., Ferguson, H. C., Giavalisco, M., et al. 2013, ApJS, 207, 24 Hopkins, P. F., Kereš, D., Oñorbe, J., et al. 2014, MNRAS, 445, 581 Illingworth, G. D., Magee, D., Oesch, P. A., et al. 2013, ApJS, 209, 6 Kauffmann, G. 2014, MNRAS, 441, 2717 Kelly, B. C. 2007, ApJ, 665, 1489 Koekemoer, A. M., Ellis, R. S., McLure, R. J., et al. 2013, ApJS, 209, 3 Koekemoer, A. M., Faber, S. M., Ferguson, H. C., et al. 2011, ApJS, Lee, N., Sanders, D. B., Casey, C. M., et al. 2015, ApJ, 801, 80 Lee, S.-K., Ferguson, H. C., Somerville, R. S., Wiklind, T., & Giavalisco, M. 2010, ApJ, 725, 1644 McQuinn, K. B. W., Skillman, E. D., Cannon, J. M., et al. 2010, ApJ, Noeske, K. G., Weiner, B. J., Faber, S. M., et al. 2007, ApJL., 660, L43 Rafelski, M., Teplitz, H. I., Gardner, J. P., et al. 2015, AJ, 150, 31 Rodriguez-Puebla, A., Primack, J. R., Behroozi, P., & Faber, S. M. 2015, ApJ, 799, 130 Salim, S., Rich, R. M., Charlot, S., et al. 2007, ApJS, 173, 267 Salmon, B., Papovich, C., Finkelstein, S. L., et al. 2015, ApJ, 799, 183 Salpeter, E. E. 1959, ApJ, 129, 608 Santini, P., Ferguson, H. C., Fontana, A., et al. 2015, ApJ, 801, 97 Shen, S., Madau, P., Conroy, C., Governato, F., & Mayer, L. 2014, ApJ, Shivaei, I., Reddy, N. A., Steidel, C. C., & Shapley, A. E. 2015, ApJ, 804, 149 Skelton, R. E., Whitaker, K. E., Momcheva, I. G., et al. 2014, ApJS, Somerville, R. S., Popping, G., & Trager, S. C. 2015, MNRAS, 453, 4337 Sparre, M., Hayward, C. C., Feldmann, R., et al. 2015a, arXiv:1510.03869 Sparre, M., Hayward, C. C., Springel, V., et al. 2015b, MNRAS, 447, 3548 Speagle, J. S., Steinhardt, C. L., Capak, P. L., & Silverman, J. D. 2014, ApJS, 214. 15 Tacchella, S., Dekel, A., Carollo, C. M., et al. 2016, MNRAS, 457, 2790

Whitaker, K. E., Franx, M., Leja, J., et al. 2014, ApJ, 795, 104 Wuyts, S., Förster Schreiber, N. M., Lutz, D., et al. 2011, ApJ, 738, 106